ACS Medicinal Chemistry Letters

pubs.acs.org/acsmedchemlett Letter

Methyl and Fluorine Effects in Novel Orally Bioavailable Keap1−Nrf2 PPI Inhibitor

Kazuki Otake,* Minoru Ubukata, Noboru Nagahashi, Naoki Ogawa, Yoshiji Hantani, Rie Hantani, Tsuyoshi Adachi, Akihiro Nomura, Keishi Yamaguchi, Mariko Maekawa, Hideaki Mamada, Takahisa Motomura, Motohide Sato, and Kazuhito Harada*

Cite This: *ACS Med. Chem. Lett.* 2023, 14, 658−665 Read Online

ACCESS | Metrics & More | Article Recommendations | Supporting Information

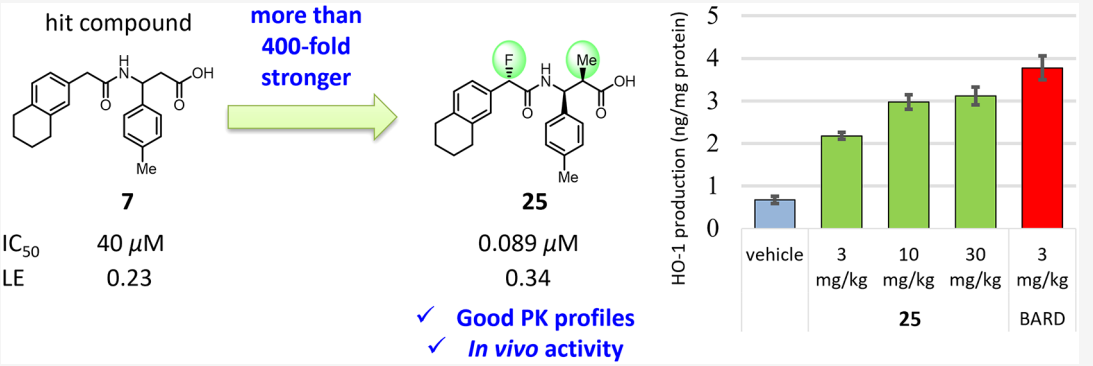

ABSTRACT: Oxidative stress is one of the causes of progression of chronic kidney disease (CKD). Activation of the antioxidant protein regulator Nrf2 by inhibition of the Keap1−Nrf2 protein−protein interaction (PPI) is of interest as a potential treatment for CKD. We report the identification of the novel and weak PPI inhibitor **7** with good physical properties by a high throughput screening (HTS) campaign, followed by structural and computational analysis. The installation of only methyl and fluorine groups successfully provided the lead compound **25**, which showed more than 400-fold stronger activity. Furthermore, these dramatic substituent effects can be explained by the analysis of using isothermal titration calorimetry (ITC). Thus, the resulting **25**, which exhibited high oral absorption and durability, would be a CKD therapeutic agent because of the dose-dependent manner for up-regulation of the antioxidant protein heme oxigenase-1 (HO-1) in rat kidneys.

KEYWORDS: *Chronic kidney disease (CKD), Keap1, Nrf2, Noncovalent inhibitor, α-Fluoramide, Binding thermodynamics*

Chronic kidney disease (CKD) is a progressive loss of kidney function, including decreased glomerular filtration rate (GFR) and the presence of albuminuria, which eventually leads to renal failure.[1] The number of CKD patients is escalating every year worldwide, and it is estimated that it will be the fifth leading cause of death by 2040.[2] Well-known risk factors for the progression of CKD comprise aging, hypertension, hyperglycemia, obesity, and oxidative stress. Current therapies for CKD include management of these risk factors and lifestyle modification (smoking cessation, salt reduction, etc.). Recently, SGLT2 inhibitors (canagloflozin,[3] dapagliflogin[4]) and the mineralocorticoid-receptor antagonist (finerenone[5]) have been approved for the treatment of CKD, but the unmet medical need for other treatments remains still high.

Nuclear factor erythroid 2-related factor 2 (Nrf2) is a transcription factor that promotes the production of approximately 250 antioxidant proteins (*heme oxygenase 1* (HO-1), NADPH quinone dehydrogenase 1 (NQO-1), etc.), and Nrf2 is believed to suppress reactive oxygen species (ROS) production and ROS-related inflammation.[6,7] Nrf2 binds to Kelch-ECH-associated protein 1 (Keap1) under basal conditions and is rapidly degraded by proteosomes via ubiquitination. On the other hand, upon exposure to oxidative stress, free Nrf2, released from binding to Keap1, is then translocated to the nucleus and promotes the production of antioxidant proteins. Bardoxolone methyl **1** (BARD, Figure 1a) is known as a Nrf2 activator that forms a covalent bond with Keap1 and significantly improved estimated glomerular filtration rate (eGFR) in patients with Stage 3−4 CKD in clinical trials.[8,9] Thus, the antioxidative approach has drawn attention as a novel CKD treatment. However, its phase 3 trial

Received: February 27, 2023
Accepted: April 5, 2023
Published: April 7, 2023

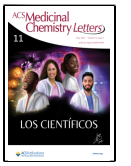

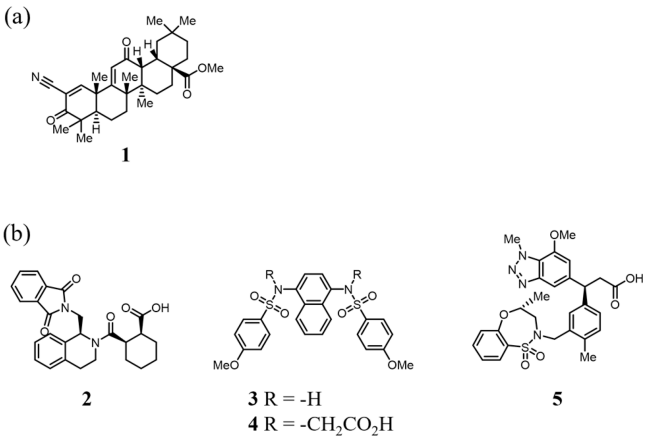

Figure 1. (a) Bardoxolone methyl (BARD). (b) Examples of published noncovalent Keap1−Nrf2 PPI inhibitors.[12a−d]

was suspended due to cardiovascular adverse events thought to be related to endothelin-mediated increases in blood pressure.[10] Due to its function as a Michael acceptor, BARD may inhibit not only Keap1 but also other cysteine-bearing molecules, and it is generally difficult to control the reactivity of covalent modifiers. Therefore, a noncovalent Nrf2 activator with reduced side effects is anticipated.

Many efforts to target inhibition of Keap1−Nrf2 protein−protein interaction (PPI) have been carried out (Figure 1b).[11,12] To date, there has been no noncovalent compound proceeding to a clinical stage. As far as we know, most of reported noncovalent compounds seem to show limited physicochemical properties[12j] such as low solubility, low metabolic stability, or low permeability, resulting in unsatisfactory bioavailability (F) and high *in vivo* clearance.[12d,g,i] To our knowledge, the best reported F value among noncovalent Keap1−Nrf2 inhibitors is 20%,[12i] except for the hydrogen peroxide responsive prodrug (F = 68%).[12h] Against such background, our goal was to identify a novel noncovalent Keap1−Nrf2 inhibitor bearing good physicochemical properties and exhibiting antioxidant effect in the kidneys. In this paper, we describe the hit identification, computational and thermodynamic analysis, *in vivo* evaluation, and medicinal chemistry efforts.

Our strategy for obtaining novel inhibitors with good physicochemical properties was (1) to select hit compounds showing high solubility and metabolic stability, and (2) to implement small structural modifications using ligand efficiency (LE) metrics[13,14] for improving the inhibitory activity while maintaining the desired properties. As a beginning of our research, high throughput screening (HTS) of our in-house chemical library was conducted using a Biacore assay, which led to the identification of two weak inhibitors (**6** and **7**) (Table 1) (manuscript on the details of the HTS campaign in preparation). From the viewpoint of metabolic stability, despite its higher lipophilicity, β-amino acid **7** showed more favorable profiles than did benzoic acid **6**. Therefore, we were interested in **7** and compared both enantiomers for inhibitory activity to confirm that (S)-enantiomer **9** was active.

To gain insight into improving the inhibitory activity of **9** by small structural modifications, X-ray crystal analysis was conducted (Figure 2a). Several interactions between **9** and

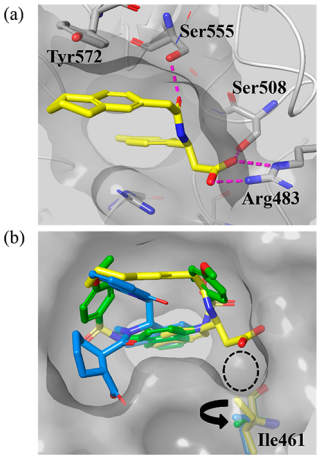

Figure 2. (a) Cocrystal structure of **9** (yellow) in the Keap1 Kelch domain. Polar interactions are depicted as dashed purple lines. (PDB 8IVG). (b) Comparison of the cocrystal structures of **9** (yellow), **2** (blue, PDB 4IFN), and **3** (green, PDB 4IQK). The surface of cocrystal structure **3** is shown to clarify a small space (dashed circle) in the binding pocket.

the Keap1 Kelch domain were observed as follows: (1) The carboxylic acid group of **9** formed a salt bridge with the side

Table 1. Hit Compounds (6, 7) and Enantiomers of 7 (8, 9)

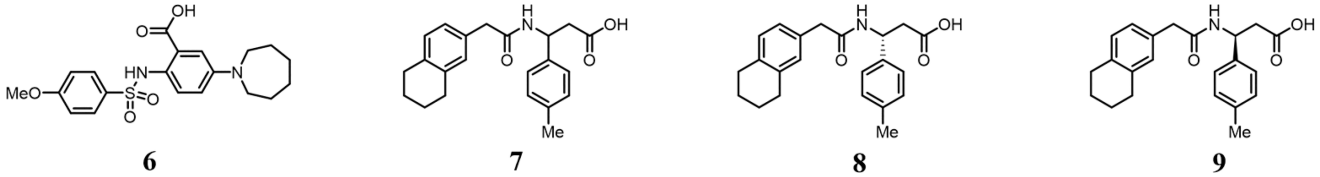

compd	IC_{50} (μM)[a]	ClogP[b]	aolubility (μM) FaSSIF	aolubility (μM) FeSSIF	Caco2 Papp (10^{-6} cm/s)	MS (% of remaining)[c] human	MS (% of remaining)[c] rat
6	37	1.38	≥475	424	13	0	0
7[d]	40	4.49	432	469	17	85	95
8	>100	4.49	[e]	[e]	[e]	[e]	[e]
9	39	4.49	[e]	[e]	[e]	[e]	[e]

[a]Values of IC_{50} are mean values determined from four replicates using a Biacore assay. Reported compound **2**[12a] was used as a positive control in each assay and gave IC_{50} (SD) = 0.71 (±0.07) μM, n = 10. [b]The ClogP value was calculated using a software from ChemAxon. [c]Metabolic stability (MS) in liver microsomes after 60 min incubation. [d]Racemate. [e]Not tested.

https://doi.org/10.1021/acsmedchemlett.3c00067
ACS Med. Chem. Lett. 2023, 14, 658−665

Table 2. SAR Exploration of the Arg483 Region

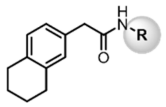

Compd	R	IC_{50} (μM)[a]	LE[b]	Compd	R	IC_{50} (μM)[a]	LE[b]
9		39	0.23	**13**	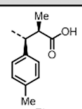	2.8	0.28
10[c]	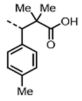	17	0.23	**14**	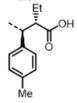	99	0.20
11[c]		54	0.21	**15**	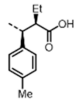	55	0.21
12	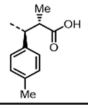	51	0.22				

[a]Values of IC_{50} are mean values determined from four replicates using a Biacore assay. Reported compound **2**[12a] was used as a positive control in each assay, and gave IC_{50} (SD) = 0.71 (±0.07) μM, n = 10. [b]LE = −1.37 log IC_{50}/number of heavy atoms. [c]Racemate.

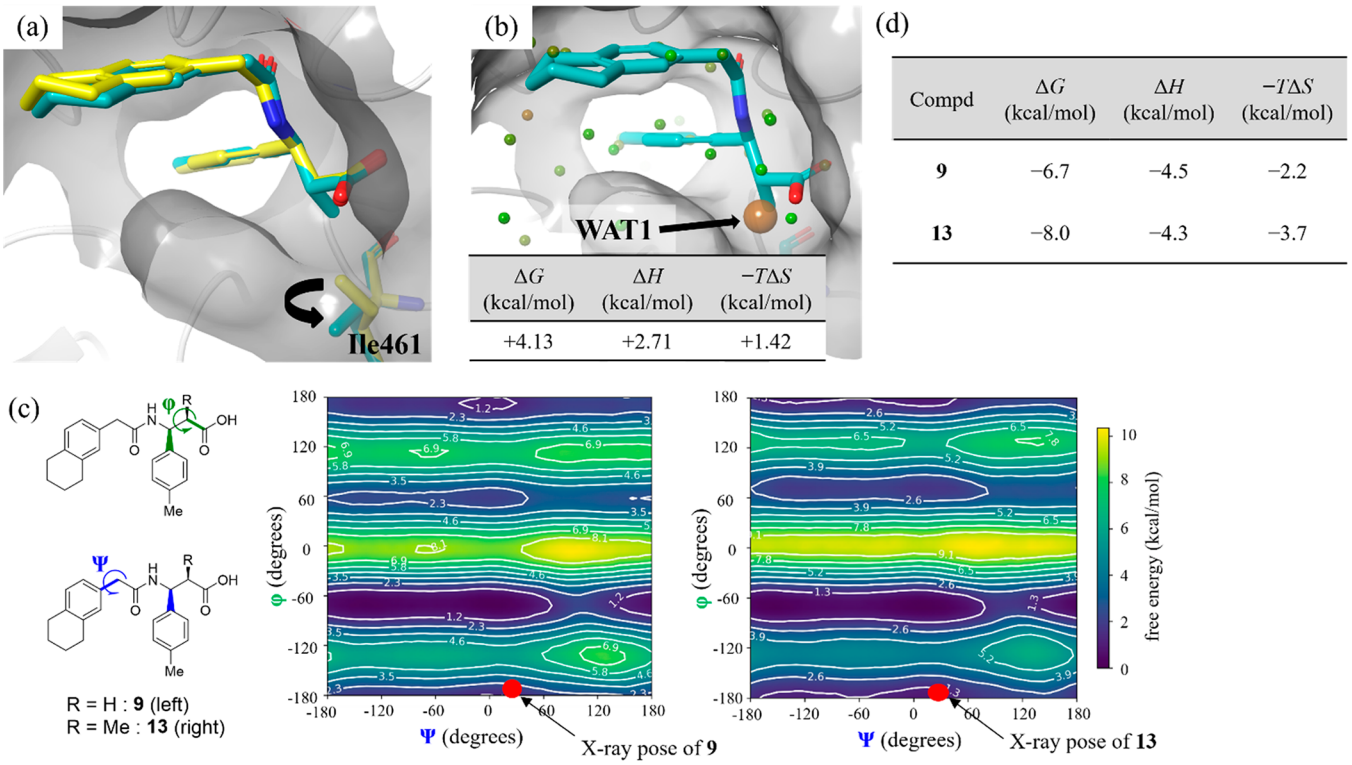

Figure 3. (a) Comparison of the cocrystal structure of **9** (yellow, PDB 8IVG) and **13** (light blue, PDB 8IVR). (b) WaterMap calculation was performed on the protein in the cocrystal structure of **13**. Detected water molecules are depicted as spheres colored according to their ΔG (green, low; orange, high). Thermodynamic profiles of WAT1 were calculated using WaterMap. (c) Two-dimensional plot of the conformational free energy surface of **9** (left) and **13** (right) constructed in the φ and ψ dihedral angles. The φ represents the rotation of the tetrahydronaphthalene and *p*-toluene. The ψ represents the rotation of the carboxylic acid and *p*-toluene. The red plot indicates the φ and ψ values observed in the cocrystal structures of **9** and **13**, respectively. (d) Thermodynamic binding parameters were measured by the ITC assay. The values are mean values determined from two replicates.

chain of Arg483, and a hydrogen bond interaction occurred with Ser508 residue. (2) The amidecarbonyl moiety of **9** made a hydrogen bond interaction with the side chain of Ser555. (3) The *p*-toluene moiety was accommodated deeply in the hydrophobic entrance to the central β-propeller tunnel. (4) The tetrahydronaphthalene unit was located in the hydrophobic region formed by the side chain of Tyr572. Next, we precisely compared the binding mode of **9** with other reported

https://doi.org/10.1021/acsmedchemlett.3c00067
ACS Med. Chem. Lett. 2023, 14, 658−665

costructures and found that in proteins such as PDBs 4IFN[15] and 4IQK,[12b] the side chain of Ile461 was moved out against the ligand, creating a small space. On the other hand, the costructure of **9** showed the side chain of Ile461 facing inward, toward the ligand (Figure 2b). This observation led us to hypothesize that the Ile461 residue might be flexible, which could trigger the creation of a new space between **9** and the protein. Moreover, we thought that the exploration of this Ile461 region would fit our strategy of increasing activity with small modifications because the region was cramped and adjacent to the ligand. Therefore, we were challenged to enhance activity by extending substituents to the region.

Table 2 showed the structure−activity relationship (SAR) result from installing small substituents at the α-position of the carboxylic acid group. In order to avoid synthetic complexity, we first investigated the installation of the *gem*-alkyl group at the position. The *gem*-dimethyl derivative **10** was about twice as potent as **9**, while conversely, the cyclopropyl one **11** was less active. Next, despite the occurrence of an additional chiral center, monoalkyl substituents at the position were tested. The (*S*)-methyl substituent (**12**) slightly decreased the activity. Conversely, the installation of the (*R*)-methyl group boosted the potency by 12-fold and enhanced the LE values (IC_{50} and LE of **13** were 2.8 and 0.28 μM, respectively). On the other hand, ethyl derivatives **14** and **15** resulted in diminished activities, suggesting that the ethyl group might be too large to fit with the Keap1 protein.

To better understand the significant increase in activity observed with the introduction of a single methyl group in **13**, structural, computational, and thermodynamic analysis were conducted. In X-ray analysis of **13**, the introduced methyl group was accommodated in the space which was created by the movement of side chain of Ile461 (Figure 3a). Next, the hydration site analysis of the Keap1 Kelch domain of the cocrystal structure with **13** was carried out by using WaterMap,[16] which is a molecular dynamics (MD)-based computational method to detect hydration sites, and also to calculate the thermodynamic properties (free energy (ΔG), enthalpy (ΔH), and entropy ($-T\Delta S$)) relative to bulk water. As shown in Figure 3b, a characteristic water molecule (WAT1) was detected as a high-energy site in the newly created space, overlapping with the introduced methyl group. Both enthalpy and entropy values of WAT1 were unstable relative to the bulk water (ΔH = 2.7 kcal/mol, $-T\Delta S$ = 1.4 kcal/mol). From this result, we thought that the WAT1 was removed by the methyl group of **13**, resulting in a hydrophobic effect. As a further analysis, a conformational energy comparison of **9** and **13** was performed (Figure 3c). The two-dimensional plot shows that the binding conformation of **13** exists in a lower energy basin than that of **9**, indicating that the methyl group also contributed to stabilizing the active conformation. Furthermore, the thermodynamic parameters of **9** and **13** were determined by isothermal titration calorimetry (ITC), which is widely used to explain ligand-protein interactions.[17−19] As shown in Figure 3d, the introduction of the methyl group decreased ΔG by 1.3 kcal/mol, which was dominated by the reduction of the entropy term ($-T\Delta S$) by 1.5 kcal/mol. In general, a value of $-T\Delta S$ is mainly affected by the hydrophobic effect and conformational change, while the components of ΔH include polar interactions, such as hydrogen bonding and van der Waals interactions.[19] Therefore, this ITC result supported the view that the increased inhibitory activity by the new methyl substituent was driven by the hydrophobic effect of removing WAT1 and stabilization of the active conformation.

Although the above significant methyl effect pleased us, the potency of **13** was not satisfactory. To further improve the activity, we compared the **13** cocrystal structure with the published inhibitor **5**, one of the most potent compounds (PDB 5FNU).[12d] Figure 4 suggested that the N atom of

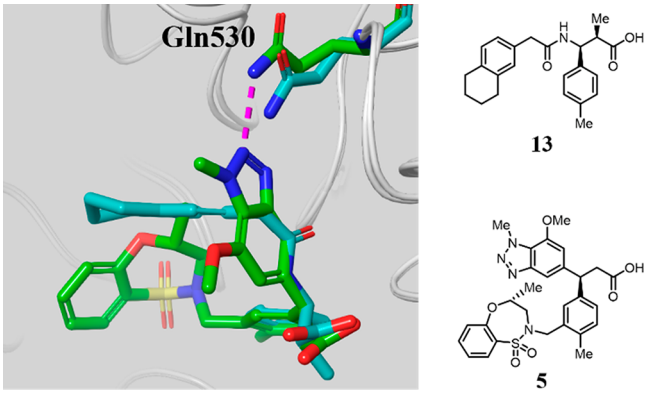

Figure 4. Comparison of the cocrystal structures of **13** (light blue, PDB 8IVR) and **5** (green, PDB 5FNU).

benzotriazole moiety in **5** made hydrogen bond interaction with the side chain of Gln530, but not in **13**. Therefore, we hypothesized that additional interaction with Gln530 would lead to a further improvement in potency. The attachment of several substituents to the benzyl position of **13** was attempted because the position was the nearest to the Gln530 residue.

In order to simplify the synthesis, compound **16** (IC_{50} = 67 μM) bearing a phenyl group instead of tetrahydronaphthalene moiety was chosen as a template to explore the Gln530 region (Table 3). The introduction of several polar groups such as carbonyl (**17**), hydroxyl (**18**, **19**), and methoxy groups (**20**, **21**) led to less potency. On the other hand, the attachment of *gem*-fluorine provided an approximately 8-fold more active compound **22**. More notably, the incorporation of chiral monofluorine resulted in a 19-fold boost in affinity and a greatly improved LE value (**16** vs **23**). Moreover, the fluorine also had a positive effect on Caco-2 permeability that differed from the carbonyl (**17**) and hydroxyl groups (**18**, **19**). This dramatic fluorine effect was also observed in the tetrahydronaphthalene derivative, and thus the obtained **25** showed the strongest inhibitory activity in our SAR study (IC_{50} = 0.089 μM). With the increase in inhibitory activity of Keap1−Nrf2 interaction, **25** exhibited higher potency in a mesangial cell assay than **13** and doubled the protein level (cell CD, Table 3) of Nrf2-regulated HO-1(heme oxygenase 1) at a dose of 2.0 μM.

With regard to the remarkable fluorine phenomenon, we also performed analyses using the X-ray, MD simulation, and ITC. The complex of **25** with the Keap1 Kelch domain revealed that the fluorine of **25** was located close to the terminal carboxamide in Gln530 with a F−N distance of 2.97 Å and functioned as a hydrogen bond acceptor (Figure 5a).[20,21] Subsequently, MD simulations were performed on the cocrystal structures of **13** and **25**, and the ligand−protein interaction frequency during the MD simulation is shown in Figure 5b. The result indicated that the amidecarbonyl moiety of **13** could not form a stable interaction with the hydroxyl group of Ser555 (Figure 5b (top), interaction frequency =

https://doi.org/10.1021/acsmedchemlett.3c00067
ACS Med. Chem. Lett. 2023, 14, 658−665

Table 3. SAR Exploration of the Gln530 Region

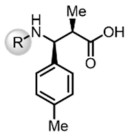

Compd	R	IC_{50} (μM)[a]	LE[b]	Cell CD (μM)[c]	Caco2 Papp (10^{-6} cm/s)	Compd	R	IC_{50} (μM)[a]	LE[b]	Cell CD (μM)[c]	Caco2 Papp (10^{-6} cm/s)
13		2.8	0.28	56	25	**21**		83	0.22	--[d]	--[d]
16		67	0.25	--[d]	2.3	**22**		8.9	0.28	66	15
17		>100	--	--[d]	1.7	**23**		3.5	0.31	36	12
18		96	0.23	--[d]	0.26	**24**		90	0.23	--[d]	6.6
19		>100	--	--[d]	0.27	**25**		0.089	0.34	2.0	33
20		>100	--	--[d]	3.4						

[a]Values of IC_{50} are mean values determined from four replicates using a Biacore assay. Reported compound **2**[12a] was used as a positive control in each assay, and gave IC_{50} (SD) = 0.71 (±0.07) μM, n = 10. [b]LE = −1.37 log IC_{50}/number of heavy atoms. [c]The concentration of compound that provoked a 2-fold increase in HO-1. Values of CD are mean values determined from two replicates. Reported compound **2**[12a] was used as a positive control in each assay, and gave CD (SD) = 10.4 (±2.3) μM, n = 5. [d]Not tested.

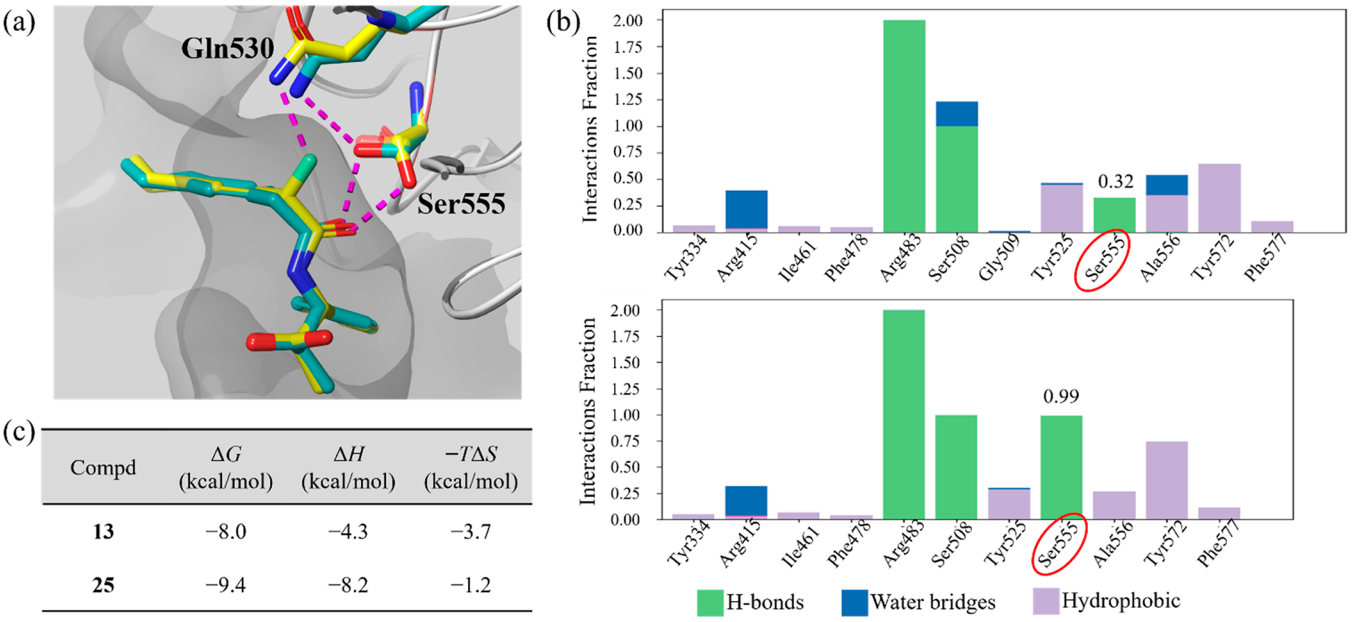

(c)

Compd	ΔG (kcal/mol)	ΔH (kcal/mol)	$-T\Delta S$ (kcal/mol)
13	−8.0	−4.3	−3.7
25	−9.4	−8.2	−1.2

Figure 5. (a) Comparison of the cocrystal structures of **13** (light blue, PDB 8IVR) and **25** (yellow, PDB 8IXS). Polar interactions are depicted as dashed purple lines. (b) Receptor−ligand interaction frequency histograms of **13** (top) and **25** (bottom) with Keap1 Kelch domain during the MD simulation. (c) Thermodynamic binding parameters were measured by the ITC assay. The values are mean values determined from two replicates.

32%), and Ser555 seemed to prefer to interact with Gln530. On the other hand, Figure 5b (bottom) showed that the amidecarbonyl moiety of **25** mostly made hydrogen bond interaction with Ser555 during the MD simulation (interaction frequency = 99%). The introduced fluorine appeared to be positioned between Gln530 and Ser555, which prevented Ser555 from approaching Gln530. These observations suggested that in addition to the gain of a new interaction with Gln530, the introduction of fluorine also strengthened the hydrogen bond interaction between the amidecarbonyl group of **25** and Ser555. As a result, these fluorine effects provided an enthalpy-driven signal in thermodynamic properties of **25** in ITC experiments (Figure 5c). In contrast, we also observed an entropy loss compared to **13**. This loss occurred seemly due to its unfavorable ligand strain of the unique active conformation with a torsion angle for F−C−C═O of 25.5° in the complex

https://doi.org/10.1021/acsmedchemlett.3c00067
ACS Med. Chem. Lett. 2023, 14, 658−665

with **25**, whereas a C−F bond is preferable to align antiparallel to a C═O bond because of the dipole repulsion.[22] Although an unfavorable entropy change was caused by the introduction of fluorine, the enthalpy gain overcompensated for this loss, resulting in an improvement in potency.

The α-fluoramide moiety in **25** may be a substructure not often seen in drug discovery.[23] However, our findings showed that it serves as a novel motif that interacts with two neighboring hydrogen bond donors without deteriorating membrane permeability, unlike other polar groups.

The best compound, **25**, in our SAR study was advanced to further characterizations and the results are shown in Figure 6a. Similar to initial compound **7**, **25** showed good solubility,

(a)

ClogP	Solubility (μM)		Caco2 Papp (10^{-6} cm/s)	MS (% of remaining)	
	FaSSIF	FeSSIF		human	rat
5.21	≧475	303	33	70	87

Rat PK			
iv (1.0 mg/kg)		po (3.0 mg/kg)	
MRT (hr)	5.6	MRT (hr)	10
$t_{1/2}$ (hr)	4.5	t_{max} (hr)	1.3
Cltot (L/hr/kg)	0.03	C_{max} (μM)	25.7
Vd (L/kg)	0.18	AUC (μM·hr)	324
AUC (μM·hr)	79	F (%)	136

(b)

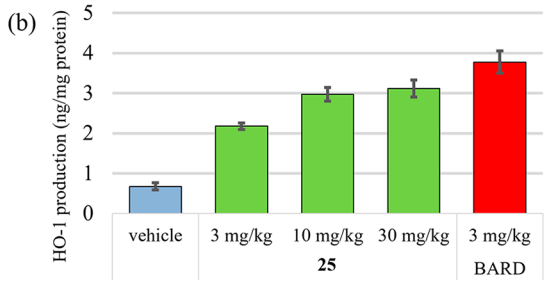

Figure 6. (a) *In vitro* profiles and *in vivo* PK result of **25**. The ClogP value was calculated using software from ChemAxon. MS: metabolic stability in liver microsomes after 60 min incubation. (b) Effect of **25** and BARD on the amounts of HO-1 proteins in kidney tissue of Wister rats at 6 h after oral administration. Error bars represent the standard error from five independent samples.

high permeability, and tolerable metabolic stability in liver microsomes of human and rat. Moreover, as expected from good *in vitro* properties, **25** exhibited desirable PK profiles including low clearance (Cl_{tot} = 0.03 L/h/kg) and high plasma exposure (AUC = 324 μM·h).[24] As far as we know, **25** has the lowest *in vivo* clearance and best bioavailability among reported Keap1−Nrf2 inhibitors.

To investigate the *in vivo* pharmacological effects, the amounts of HO-1 proteins in kidney tissue in Wistar rats at 6 h after orally administration of **25** were measured. As shown in Figure 6b, a dose dependent increase in the protein level of HO-1 was observed. In this experiment, 30 mg/kg dosing of **25** led to a 4.6 fold increase over vehicle controls, which was comparable to 3 mg/kg of BARD, a well-known covalent Nrf2 activator undergoing clinical trials. This result demonstrated that the inhibition of Nrf2−Keap1 interaction with our novel noncovalent inhibitor resulted in an increase in oxidative stress suppressor proteins in kidneys.

Representative compound **25** was synthesized according to Scheme 1 (synthetic routes of other compounds are shown in

Scheme 1. Synthesis of 25[a]

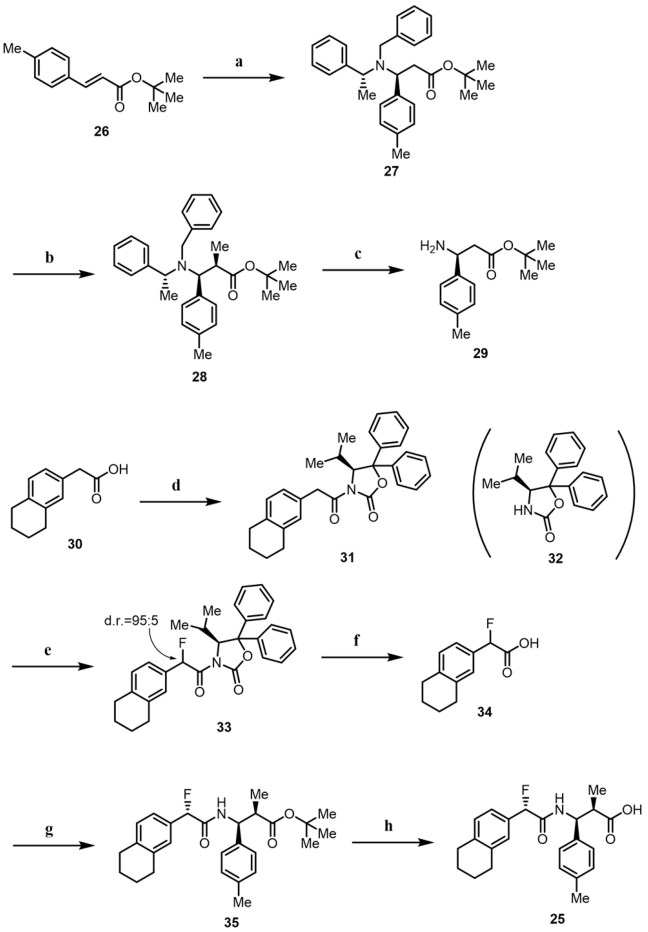

[a]Reagents and conditions: (a) (*R*)-*N*-benzyl-1-phenylethan-1-amine, *n*-BuLi, THF, −78 °C, 98%; (b) LDA, iodomethane, THF, −78 °C, 71%; (c) H_2, $Pd(OH)_2/C$, MeOH, rt, 98%; (d) (i) pivaloyl chloride, Et_3N, THF, −78 to 0 °C; (ii) **32**, *n*-BuLi, THF, −78 to 0 °C, 81% over 2 steps; (e) LDA, *N*-fluorobenzenesulfonimide, THF, −78 to 0 °C, 82%; (f) 30% H_2O_2 aq, $LiOH·H_2O$, THF, H_2O, rt; (g) **29**, EDC, HOBt, DMF, rt, 82% over 2 steps; (h) HCl, 1,4-dioxane, rt, 98%.

the Supporting Information). To prepare chiral β-amino-ester **29**, starting from *tert*-butyl-cinnamate **26**, the conjugate addition of (*R*)-*N*-benzyl-1-phenylethan-1-amine gave *tert*-butyl β-amino ester **27** as a single diastereomer according to the procedure developed by Davies.[25] Highly diastereoselective methylation of the resulting **27** with LDA and iodomethane afforded adduct **28**. Hydrogenation in the presence of $Pd(OH)_2/C$ was then carried out to obtain **29**. For the preparation of α-fluorocarboxylic acid **34**, chiral imide **31** was initially prepared by coupling of phenylacetic acid **30** with chiral oxazolidinone **32**. Treatment of **31** with NFSI under basic conditions and subsequent slurry purification yielded fluorinated imide **33** as a mixture of diastereomers (dr = 95:5). The removal of the chiral auxiliary on treatment with LiOOH (formed *in situ*) led to α-fluorocarboxylic acid **34**, which was coupled with β-amino ester **29** followed by silicagel chromatography separation to afford condensate **35** as a single

https://doi.org/10.1021/acsmedchemlett.3c00067
ACS Med. Chem. Lett. 2023, 14, 658−665

isomer. Finally, *tert*-butyl ester **35** was treated with HCl to give **25**. The stereochemistry of **25** was presumed from the cocrystal structure with Keap1.

In conclusion, we have described the discovery of novel noncovalent Nrf2−Keap1 inhibitors. We conducted a HTS campaign and identified hit compound **7** which showed good physicochemical properties. The SBDD approach contributed to the efficient drug discovery, and small modifications with methyl and fluoro group incorporation provided **25** with approximately 450-fold more potent inhibition than **7** while maintaining favorable *in vitro* ADME profiles. In addition, we analyzed the enhancement of activity using computational studies (WaterMap, conformational analysis and MD simulations) and ITC experiments and found the unique binding mode and new use of the α-fluoramide moiety. Most gratifyingly, **25** displayed robust PK profiles and *in vivo* potency, which demonstrated that **25** would be a useful chemical tool for investigating the treatment for CKD. Further efforts to improve *in vivo* potency will be described in the next report.

■ ASSOCIATED CONTENT

Supporting Information

The Supporting Information is available free of charge at https://pubs.acs.org/doi/10.1021/acsmedchemlett.3c00067.

Synthetic schemes, procedures, experimental data of all compounds, and assay procedures (PDF)

■ AUTHOR INFORMATION

Corresponding Authors

Kazuki Otake − *Central Pharmaceutical Research Institute, Japan Tobacco Inc., Takatsuki 569-1125 Osaka, Japan;* orcid.org/0009-0006-1225-5133; Phone: +81-72-681-9700; Email: kazuki.otake@jt.com

Kazuhito Harada − *Central Pharmaceutical Research Institute, Japan Tobacco Inc., Takatsuki 569-1125 Osaka, Japan;* orcid.org/0009-0009-5429-9486; Phone: +81-72-681-9700; Email: kazuhito.harada@jt.com

Authors

Minoru Ubukata − *Central Pharmaceutical Research Institute, Japan Tobacco Inc., Takatsuki 569-1125 Osaka, Japan*

Noboru Nagahashi − *Central Pharmaceutical Research Institute, Japan Tobacco Inc., Takatsuki 569-1125 Osaka, Japan*

Naoki Ogawa − *Central Pharmaceutical Research Institute, Japan Tobacco Inc., Takatsuki 569-1125 Osaka, Japan*

Yoshiji Hantani − *Central Pharmaceutical Research Institute, Japan Tobacco Inc., Takatsuki 569-1125 Osaka, Japan;* orcid.org/0000-0002-7010-2470

Rie Hantani − *Central Pharmaceutical Research Institute, Japan Tobacco Inc., Takatsuki 569-1125 Osaka, Japan*

Tsuyoshi Adachi − *Central Pharmaceutical Research Institute, Japan Tobacco Inc., Takatsuki 569-1125 Osaka, Japan*

Akihiro Nomura − *Central Pharmaceutical Research Institute, Japan Tobacco Inc., Takatsuki 569-1125 Osaka, Japan*

Keishi Yamaguchi − *Central Pharmaceutical Research Institute, Japan Tobacco Inc., Takatsuki 569-1125 Osaka, Japan*

Mariko Maekawa − *Central Pharmaceutical Research Institute, Japan Tobacco Inc., Takatsuki 569-1125 Osaka, Japan*

Hideaki Mamada − *Central Pharmaceutical Research Institute, Japan Tobacco Inc., Takatsuki 569-1125 Osaka, Japan;* orcid.org/0000-0002-5433-7042

Takahisa Motomura − *Central Pharmaceutical Research Institute, Japan Tobacco Inc., Takatsuki 569-1125 Osaka, Japan*

Motohide Sato − *Central Pharmaceutical Research Institute, Japan Tobacco Inc., Takatsuki 569-1125 Osaka, Japan*

Complete contact information is available at: https://pubs.acs.org/10.1021/acsmedchemlett.3c00067

Notes

The authors declare no competing financial interest.

■ ACKNOWLEDGMENTS

We thank Takahiro Iwai for single-crystal X-ray structure analysis, Eita Nagao for HRMS analysis, and Mitsumasa Takahashi for ^{13}C NMR analysis. We are also grateful to Dr. Makoto Shiozaki for helpful suggestions.

■ ABBREVIATIONS

CKD, chronic kidney disease; Keap1, Kelch-ECH-associated protein 1; DMF, *N*,*N*-dimethylformamide; dr, diastereomeric ratio; EDC, 1-ethyl-3-(3-(dimethylamino)propyl)carbodiimide hydrochloride; GFR, glomerular filtration rate; HO-1, heme oxygenase 1; HOBt, 1-hydroxybenzotriazole hydrate; ITC, isothermal titration calorimetry; LDA, lithium diisopropylamide; MD, molecular dynamics; Nrf2, nuclear factor erythroid 2-related factor 2; NQO1, NAD(P)H quinone dehydrogenase 1; PK, pharmacokinetics; PPI, protein−protein interaction; SAR, structure−activity relationship; SBDD, structure-based drug design; THF, tetrahydrofuran

■ REFERENCES

(1) Jager, K. J.; Kovesdy, C.; Langham, R.; Rosenberg, M.; Jha, V.; Zoccali, C. A single number for advocacy and communication-worldwide more than 850 million individuals have kidney diseases. *Kidney Int.* **2019**, *96*, 1048−1050.

(2) Foreman, K. J.; Marquez, N.; Dolgert, A.; Fukutaki, K.; Fullman, N.; McGaughey, M.; Pletcher, M. A.; Smith, A. E.; Tang, K.; Yuan, C.-W.; Brown, J. C.; Friedman, J.; He, J.; Heuton, K. R.; Holmberg, M.; Patel, D. J.; Reidy, P.; Carter, A.; Cercy, K.; Chapin, A.; Douwes-Schultz, D.; Frank, T.; Goettsch, F.; Liu, P. Y.; Nandakumar, V.; Reitsma, M. B.; Reuter, V.; Sadat, N.; Sorensen, R. J. D.; Srinivasan, V.; Updike, R. L.; York, H.; Lopez, A. D.; Lozano, R.; Lim, S. S.; Mokdad, A. H.; Vollset, S. E.; Murray, C. J. L. Forecasting life expectancy, years of life lost, and all-cause and cause-specific mortality for 250 causes of death: reference and alternative scenarios for 2016−40 for 195 countries and territories. *Lancet.* **2018**, *392*, 2052−2090.

(3) Perkovic, V.; Jardine, M. J.; Neal, B.; Bompoint, S.; Heerspink, H. J. L.; Charytan, D. M.; Edwards, R.; Agarwal, R.; Bakris, G.; Bull, S.; Cannon, C. P.; Capuano, G.; Chu, P.-L.; de Zeeuw, D.; Greene, T.; Levin, A.; Pollock, C.; Wheeler, D. C.; Yavin, Y.; Zhang, H.; Zinman, B.; Meininger, G.; Brenner, B. M.; Mahaffey, K. W. Canagliflozin and renal outcomes in type 2 diabetes and nephropathy. *N. Engl. J. Med.* **2019**, *380*, 2295−2306.

(4) Heerspink, H. J. L.; Stefánsson, B. V.; Correa-Rotter, R.; Chertow, G. M.; Greene, T.; Hou, F.-F.; Mann, J. F. E.; McMurray, J. J. V.; Lindberg, M.; Rossing, P.; Sjöström, C. D.; Toto, R. D.; Langkilde, A.-M.; Wheeler, D. C. Dapagliflozin in patients with chronic kidney disease. *N. Engl. J. Med.* **2020**, *383*, 1436−1446.

(5) Bakris, G. L.; Agarwal, R.; Anker, S. D.; Pitt, B.; Ruilope, L. M.; Rossing, P.; Kolkhof, P.; Nowack, C.; Schloemer, P.; Joseph, A.; Filippatos, G. Effect of finerenone on chronic kidney disease outcomes in type 2 diabetes. *N. Engl. J. Med.* **2020**, *383*, 2219−2229.

(6) Itoh, K.; Wakabayashi, N.; Katoh, Y.; Ishii, T.; Igarashi, K.; Engel, J. D.; Yamamoto, M. Keap1 represses nuclear activation of antioxidant responsive elements by Nrf2 through binding to the amino-terminal Neh2 domain. *Genes Dev.* **1999**, *13*, 76−86.
(7) Kobayashi, A.; Kang, M. I.; Okawa, H.; Ohtsuji, M.; Zenke, Y.; Chiba, T.; Igarashi, K.; Yamamoto, M. Oxidative stress sensor Keap1 functions as an adaptor for Cul3-based E3 ligase to regulate proteasomal degradation of Nrf2. *Mol. Cell. Biol.* **2004**, *24*, 7130−7139.
(8) Pergola, P. E.; Raskin, P.; Toto, R. D.; Meyer, C. J.; Huff, J. W.; Grossman, E. B.; Krauth, M.; Ruiz, S.; Audhya, P.; Christ-Schmidt, H.; Wittes, J.; Warnock, D. G. Bardoxolone methyl and kidney function in CKD with type 2 diabetes. *N. Engl. J. Med.* **2011**, *365*, 327−336.
(9) de Zeeuw, D.; Akizawa, T.; Audhya, P.; Bakris, G. L.; Chin, M.; Christ-Schmidt, H.; Goldsberry, A.; Houser, M.; Krauth, M.; Lambers Heerspink, H. J.; McMurray, J. J.; Meyer, C. J.; Parving, H.-H.; Remuzzi, G.; Toto, R. D.; Vaziri, N. D.; Wanner, C.; Wittes, J.; Wrolstad, D.; Chertow, G. M. Bardoxolone methyl in type 2 diabetes and stage 4 chronic kidney disease. *N. Engl. J. Med.* **2013**, *369*, 2492−2503.
(10) Chin, M. P.; Reisman, S. A.; Bakris, G. L.; O'Grady, M.; Linde, P. G.; McCullough, P. A.; Packham, D.; Vaziri, N. D.; Ward, K. W.; Warnock, D. G.; Meyer, C. J. Mechanisms contributing to adverse cardiovascular events in patients with type 2 diabetes mellitus and stage 4 chronic kidney disease treated with bardoxolone methyl. *Am. J. Nephrol.* **2014**, *39*, 499−508.
(11) Recent review articles of Keap1−Nrf2 inhibitors: (a) Mou, Y.; Wen, S.; Li, T.-X.; Gao, X.-X.; Zhang, X.; Jiang, Z.-Y. Recent progress in Keap1-Nrf2 protein-protein interaction inhibitors. *Eur. J. Med. Chem.* **2020**, *202*, 112532. (b) Crisman, E.; Duarte, P.; Dauden, E.; Cuadrado, A.; Rodriguez-Franco, M. I.; Lopez, M. G.; Leon, R. Keap1-Nrf2 protein-protein interaction inhibitors: Design, pharmacological properties and therapeutic potential. *Med. Res. Rev.* **2023**, *43*, 237−287.
(12) Some examples of noncovalent Keap1−Nrf2 inhibitors are listed: (a) Hu, L.; Magesh, S.; Chen, L.; Wang, L.; Lewis, T. A.; Chen, Y.; Khodier, C.; Inoyama, D.; Beamer, L. J.; Emge, T. J.; Shen, J.; Kerrigan, J. E.; Kong, A. N.; Dandapani, S.; Palmer, M.; Schreiber, S. L.; Munoz, B. Discovery of a small-molecule inhibitor and cellular probe of Keap1-Nrf2 protein-protein interaction. *Bioorg. Med. Chem. Lett.* **2013**, *23*, 3039−3043. (b) Marcotte, D.; Zeng, W.; Hus, J. C.; McKenzie, A.; Hession, C.; Jin, P.; Bergeron, C.; Lugovskoy, A.; Enyedy, I.; Cuervo, H.; Wang, D.; Atmanene, C.; Roecklin, D.; Vecchi, M.; Vivat, V.; Kraemer, J.; Winkler, D.; Hong, V.; Chao, J.; Lukashev, M.; Silvian, L. Small molecules inhibit the interaction of Nrf2 and the Keap1 Kelch domain through a non-covalent mechanism. *Bioorg. Med. Chem.* **2013**, *21*, 4011−4019. (c) Jiang, Z. Y.; Lu, M. C.; Xu, L. L.; Yang, T. T.; Xi, M. Y.; Xu, X. L.; Guo, X. K.; Zhang, X. J.; You, Q. D.; Sun, H. P. Discovery of potent Keap1-Nrf2 protein-protein interaction inhibitor based on molecular binding determinants analysis. *J. Med. Chem.* **2014**, *57*, 2736−2745. (d) Davies, T. G.; Wixted, W. E.; Coyle, J. E.; Griffiths-Jones, C.; Hearn, K.; McMenamin, R.; Norton, D.; Rich, S. J.; Richardson, C.; Saxty, G.; Willems, H. M.; Woolford, A. J.; Cottom, J. E.; Kou, J. P.; Yonchuk, J. G.; Feldser, H. G.; Sanchez, Y.; Foley, J. P.; Bolognese, B. J.; Logan, G.; Podolin, P. L.; Yan, H.; Callahan, J. F.; Heightman, T. D.; Kerns, J. K. Monoacidic inhibitors of the Kelch-like ECH-associated protein 1: nuclear factor erythroid 2-related factor 2 (KEAP1:NRF2) protein-protein interaction with high cell potency identified by fragment-based discovery. *J. Med. Chem.* **2016**, *59*, 3991−4006. (e) Richardson, B. G.; Jain, A. D.; Potteti, H. R.; Lazzara, P. R.; David, B. P.; Tamatam, C. R.; Choma, E.; Skowron, K.; Dye, K.; Siddiqui, Z.; Wang, Y. T.; Krunic, A.; Reddy, S. P.; Moore, T. W. Replacement of a naphthalene scaffold in Kelch-like ECH-associated protein 1 (KEAP1)/nuclear factor (erythroid-derived 2)-like 2 (NRF2) inhibitors. *J. Med. Chem.* **2018**, *61*, 8029−8047. (f) Abed, D. A.; Lee, S.; Hu, L. Discovery of disubstituted xylylene derivatives as small molecule direct inhibitors of Keap1-Nrf2 protein-protein interaction. *Bioorg. Med. Chem.* **2020**, *28*, 115343. (g) Ma, B.; Lucas, B.; Capacci, A.; Lin, E. Y.; Jones, J. H.; Dechantsreiter, M.; Enyedy, I.; Marcotte, D.; Xiao, G.; Li, B.; Richter, K. Design, synthesis and identification of novel, orally bioavailable non-covalent Nrf2 activators. *Bioorg. Med. Chem. Lett.* **2020**, *30*, 126852. (h) Lu, M.; Zhang, X.; Zhao, J.; You, Q.; Jiang, Z. A hydrogen peroxide responsive prodrug of Keap1-Nrf2 inhibitor for improving oral absorption and selective activation in inflammatory conditions. *Redox Biol.* **2020**, *34*, 101565. (i) Liu, G.; Hou, R.; Xu, L.; Zhang, X.; Yan, J.; Xing, C.; Xu, K.; Zhuang, C. Crystallography-guided optimizations of the Keap1-Nrf2 inhibitors on the solvent exposed region: from symmetric to asymmetric naphthalenesulfonamides. *J. Med. Chem.* **2022**, *65*, 8289−8302. (j) Georgakopoulos, N.; Talapatra, S.; Dikovskaya, D.; Dayalan Naidu, S.; Higgins, M.; Gatliff, J.; Ayhan, A.; Nikoloudaki, R.; Schaap, M.; Valko, K.; Javid, F.; Dinkova-Kostova, A. T.; Kozielski, F.; Wells, G. Phenyl bis-sulfonamide Keap1-Nrf2 protein−protein interaction inhibitors with an alternative binding mode. *J. Med. Chem.* **2022**, *65*, 7380−7398. (k) Narayanan, D.; Tran, K. T.; Pallesen, J. S.; Solbak, S. M. Ø.; Qin, Y.; Mukminova, E.; Luchini, M.; Vasilyeva, K. O.; Gonzalez Chichon, D.; Goutsiou, G.; Poulsen, C.; Haapanen, N.; Popowicz, G. M.; Sattler, M.; Olagnier, D.; Gajhede, M.; Bach, A. Development of noncovalent small-molecule Keap1-Nrf2 inhibitors by fragment-based drug discovery. *J. Med. Chem.* **2022**, *65*, 14481−14526.
(13) Kuntz, I. D.; Chen, K.; Sharp, K. A.; Kollman, P. A. The maximal affinity of ligands. *Proc. Natl. Acad. Sci. U. S. A.* **1999**, *96*, 9997−10002.
(14) Hopkins, A. L.; Groom, C. R.; Alex, A. Ligand efficiency: a useful metric for lead selection. *Drug Discovery Today* **2004**, *9*, 430−431.
(15) Jnoff, E.; Albrecht, C.; Barker, J. J.; Barker, O.; Beaumont, E.; Bromidge, S.; Brookfield, F.; Brooks, M.; Bubert, C.; Ceska, T.; Corden, V.; Dawson, G.; Duclos, S.; Fryatt, T.; Genicot, C.; Jigorel, E.; Kwong, J.; Maghames, R.; Mushi, I.; Pike, R.; Sands, Z. A.; Smith, M. A.; Stimson, C. C.; Courade, J. P. Binding mode and structure-activity relationships around direct inhibitors of the Nrf2-Keap1 complex. *ChemMedChem.* **2014**, *9*, 699−705.
(16) Abel, R.; Young, T.; Farid, R.; Berne, B. J.; Friesner, R. A. Role of the active-site solvent in the thermodynamics of Factor Xa ligand binding. *J. Am. Chem. Soc.* **2008**, *130*, 2817−2831.
(17) Klebe, G. Applying thermodynamic profiling in lead finding and optimization. *Nat. Rev. Drug. Discovery* **2015**, *14*, 95−110.
(18) Nasiri, H. R.; Linge, S.; Ullmann, D. Thermodynamic profiling of inhibitors of Nrf2: Keap1 interactions. *Bioorg. Med. Chem. Lett.* **2016**, *26*, 526−529.
(19) Liu, W.; Jiang, J.; Lin, Y.; You, Q.; Wang, L. Insight into thermodynamic and kinetic profiles in small-molecule optimization. *J. Med. Chem.* **2022**, *65*, 10809−10847.
(20) Howard, J. A. K.; Hoy, V. J.; O'Hagan, D.; Smith, G. T. How good is fluorine as a hydrogen bond acceptor? *Tetrahedron* **1996**, *52*, 12613−12622.
(21) Hagmann, W. K. The many roles for fluorine in medicinal chemistry. *J. Med. Chem.* **2008**, *51*, 4359−4369.
(22) Winkler, M.; Moraux, T.; Khairy, H. A.; Scott, R. H.; Slawin, A. M. Z.; O'Hagan, D. Synthesis and vanilloid receptor (TRPV1) activity of the enantiomers of α-fluorinated capsaicin. *ChemBioChem.* **2009**, *10*, 823−828.
(23) The number of cocrystals of compounds bearing acyclic α-fluoramides reported in Protein Data Bank are less than 10.
(24) The po dose was higher than the iv dose, and it is possible that compound **25** exhibited saturable metabolism in liver after po administration. Therefore, the AUC might increase nonlinearly, and the oral bioavailability exceeded 100%.
(25) Davies, S. G.; Smith, A. D.; Price, P. D. The conjugate addition of enantiomerically pure lithium amides as homochiral ammonia equivalents: scope, limitations and synthetic applications. *Tetrahedron Asymmetry* **2005**, *16*, 2833−2891.

https://doi.org/10.1021/acsmedchemlett.3c00067
ACS Med. Chem. Lett. 2023, 14, 658−665